Dynamin-2 Mutations Linked to Neonatal-onset Centronuclear Myopathy impair exocytosis and endocytosis in adrenal chromaffin cells.

Lucas Bayonés[1 §], María José Guerra-Fernández[2], Cindel Figueroa-Cares[2], Luciana I. Gallo[1], Samuel Alfonso-Bueno[1], Ximena Báez-Matus[2], Arlek González-Jamett[2,3], Ana M. Cárdenas[2 *] and Fernando D. Marengo[1 *]

[1]Instituto de Fisiología, Biología Molecular y Neurociencias. CONICET. Departamento de Fisiología y Biología Molecular y Celular. Facultad de Ciencias Exactas y Naturales. Universidad de Buenos Aires, Buenos Aires, 1428, Argentina.
[2]Centro Interdisciplinario de Neurociencia de Valparaíso, Facultad de Ciencias, Universidad de Valparaíso, Gran Bretaña 1111, Valparaíso, 2360102, Chile.
[3]Escuela de Química y Farmacia, Facultad de Farmacia, Universidad de Valparaíso, Valparaíso 2360102, Chile.

* Address for correspondence:

Fernando D. Marengo
Instituto de Fisiología, Biología Molecular y Neurociencias
Ciudad Universitaria. Buenos Aires, Argentina (PC: 1428)
TEL: +54-11-4576-3368 - FAX: +54-11-4576-3321 - E-mail: fernando@fbmc.fcen.uba.ar

Ana María Cárdenas
Gran Bretaña 1111, Valparaíso, Chile (PC: 2360102)
TEL: +56 32 2508052. E-MAIL: ana.cardenas@uv.cl

§ Lucas Bayonés present address: Instituto de Fisiología Celular, División de Neurociencias, Ciudad Universitaria, Coyoacán, 04510 Ciudad de México, CDMX. Mail to: lbayones@ifc.unam.mx

Abbreviations: Anti-Dyn, monoclonal antibody against dynamin 1 and 2; APls, action potential-like stimulus; Cm, cell capacitance; ΔCm_{endo}, decrease in Cm; ΔCm_{exo}, synchronous increase in Cm; CNM, centronuclear myopathy; DMPP: 1,1-dimethyl-4-phenyl piperazine iodide; EGFP, green fluorescent protein; HAT, time elapsed at amperometric spike half amplitude; $I_{Ca^{2+}}$, calcium current amplitude; $\int I_{Ca^{2+}}$; calcium current integral; nAChRs, nicotinic acetylcholine receptors; NPY, neuropeptide Y; NPY-mCherry, Neuropeptide Y linked to mCherry; PBS, phosphate buffer saline; PH, pleckstrin homology domain; PRD, proline-rich domain; PSF, pre-spike foot signal; Q, amperometric spike charge; ΣQ, cumulative Q along experimental time; τ_{endo}, endocytosis time constant; WT: wild type.

ABSTRACT

Dynamins are large GTPases whose primary function is to catalyze membrane scission during endocytosis, but also modulate other cellular processes, such as actin polymerization and vesicle trafficking. Recently, we reported that centronuclear myopathy associated dynamin-2 mutations, p.A618T and p.S619L, impair Ca^{2+}-induced exocytosis of GLUT4 containing vesicles in immortalized human myoblasts. As exocytosis and endocytosis occur within rapid timescales, here we applied high-temporal resolution techniques, such as patch-clamp capacitance measurements and carbon-fiber amperometry to assess the effects of these mutations on these two cellular processes using bovine chromaffin cells as a study model. We found that the expression of any of these dynamin-2 mutants inhibits a dynamin and F-actin dependent form of fast endocytosis triggered by single action potential stimulus, as well as inhibits a slow compensatory endocytosis induced by 500 ms square depolarization. Both dynamin-2 mutants further reduced the exocytosis induced by 500 ms depolarizations, and the frequency of release events and the recruitment of NPY-labelled vesicles to the cell cortex after stimulation of nicotinic acetylcholine receptors with DMPP. They also provoked a significant decrease in the Ca^{2+}-induced formation of new actin filaments in permeabilized chromaffin cells. In summary, our results indicate that the CNM-linked p.A618T and p.S619L mutations in dynamin-2 affect exocytosis and endocytosis, being the disruption of F-actin a possible explanation for these results. These impaired cellular processes might underlie the pathogenic mechanisms associated with these mutations.

INTRODUCTION

Dynamins are a family of large GTPases that form high-order homo-oligomers and play pivotal roles in various cellular processes. These proteins consist of distinct domains, including a GTPase domain, a stalk region involved in self-assembly, a bundle signaling element (BSE) module that connects the G-domain with the stalk and transmits conformational changes upon GTP hydrolysis, a pleckstrin homology domain (PH) for membrane binding, and a proline-rich domain (PRD) (Arriagada-Diaz et al., 2020). Their primary function involves catalyzing membrane scission during clathrin-mediated endocytosis, caveolae internalization, and membrane budding (Arriagada-Diaz et al., 2020). Furthermore, dynamins are key regulators of cytoskeletal actin remodeling, contributing to diverse mechanical actions during cellular processes, such as bulk endocytosis, phagosome formation, neuronal growth cone dynamics, membrane protrusion, and fusion pore regulation (Yamada et al., 2016a; Chuang et al., 2019; Zhang et al., 2020; González-Jamett et al., 2013a; Shin et al., 2018; Linadu and Álvarez de Toledo et al., 2003).

Among the three dynamin isoforms expressed in mammals, dynamin-2 stands out as the ubiquitous variant (González-Jamett et al., 2014). Mutations in the gene encoding dynamin-2 have been associated with two distinct neurological disorders, centronuclear myopathy (CNM) and Charcot-Marie-Tooth neuropathy (González-Jamett et al., 2013b; Ge et al., 2016). Notably, Charcot-Marie-Tooth-associated mutations predominantly affect the lipid-binding pocket within the PH domain's N-terminal region, impairing dynamin's affinity for lipids and disrupting clathrin-mediated endocytosis (González-Jamett et al., 2014; Koutsopoulos et al., 2011; Sidiropoulos et al., 2012). Conversely, CNM-associated mutations cluster in the middle domain, a region critical for oligomerization, or at the interface between the stalk region and the PH domain that coordinates lipid binding and GTPase activity (Ramachandran et al., 2007; Kenniston and Lemmon, 2010). These mutations often enhance dynamin-2 self-assembly, resulting in stable oligomers and heightened basal GTPase activity (Wang et al., 2010; Chin et al., 2015). Particularly noteworthy, the p.A618T and p.S619L mutations, located in the C-terminal α-helix motif of the PH domain, enhance lipid-stimulated GTPase

activity and basal GTPase activity, respectively (Kenniston and Lemmon, 2010). Strikingly, these two mutations have been linked to severe neonatal forms of CNM (Böhm et al., 2012).

Dynamin-2's canonical function lies in endocytosis, a process occurring within rapid timescales, necessitating high-temporal resolution techniques for accurate assessment (Chanaday and Kavalali, 2018; Montenegro et al, 2021). Therefore, to investigate the impact of p.A618T and p.S619L mutations on endocytosis, we employed capacitance measurements in patch-clamped adrenal chromaffin cells. Our findings revealed that both mutants significantly diminished fast dynamin-dependent endocytosis induced by short-term depolarization stimuli and the slow compensatory endocytosis induced by 500 ms square depolarization. Moreover, these mutations impaired the exocytosis triggered by 500 ms depolarizations, and the release events and recruitment of NPY-labelled vesicles to the cell cortex induced by stimulation of nicotinic acetylcholine receptors (nAChRs) with the agonist 1,1-dimethyl-4-phenyl piperazine iodide (DMPP). Notably, both mutations caused substantial disruptions of F-actin formation, as visualized through confocal microscopy of fluorescently-tagged G-actin. Consequently, both CNM-associated mutations adversely affected exocytosis and endocytosis, and these processes can be potentially attributed to dysregulated cytoskeletal actin filaments. These aberrant cellular processes might underlie the pathogenic mechanisms associated with these mutations.

MATERIAL AND METHODS

Plasmids

Wild type (WT) dynamin-2 fused to enhanced green fluorescent protein (EGFP) N1 rat was kindly provided by Dr. Stephane Gasman (CNRS, Strasbourg, France). The mCherry WT-dynamin-2 was constructed by GenScript Corporation (Nanjing, China) by cloning the rat dynamin-2 isoform aa (Genbank L25605) into an mCherry_pcDNA3.1(+) vector. The EGFP and mCherry dynamin-2 mutations A618T and S619L were constructed by site-directed mutagenesis using the QuikChange II XL Site-Directed Mutagenesis Kit (Agilent Technologies, Santa Clara, CA, USA). Neuropeptide Y fused to mCherry (NPY-mCherry) was kindly provided by Sebastian Barg (Gandasi et al, 2015, doi: 10.1371/journal.pone.0127801)

Chromaffin cell culture and transfections

Bovine adrenal glands were acquired from local slaughterhouses (Frigorífico Cocarsa-Ecocarnes S.A., San Fernando, Provincia de Buenos Aires, Argentina, and Frigorífico Don Pedro, Quilpué, Chile). The isolation and culture of chromaffin cells was performed as previously published (Guerra et al., 2019). In brief, after adrenal medulla digestion with a solution containing 0.25% collagenase B, 0.01% trypsin inhibitor and 0.5% bovine serum albumin, chromaffin cells were isolated by Percoll gradient centrifugation and resuspended in a 1:1 mixture of Dulbecco's Modified Eagle's Medium/Nutrient Ham's Mixture supplemented with 10% fetal bovine serum. The transfection of chromaffin cells with the plasmids described above was performed by electroporation in an Amaxa Nucleofector 4D (Lonza, Cologne, Germany) according to the manufacturer's instructions. The cells were cultured at a density of 3×10^5 cells/ml on 0.01% poly-l-lysine treated coverslips and kept at 37°C in a 5% CO2 atmosphere. Cells were used between 2 days after transfections.

Whole Cell Patch-Clamp and Membrane Capacitance Measurements

These experiments were performed in an inverted microscope (Olympus IX71, Olympus, Japan), using a patch-clamp amplifier (EPC10 double patch clamp amplifier, Heka Elektronik, Lambrecht, Germany). The application of the stimulation protocols and the acquisition of data were controlled by the Patchmaster® software (Heka, Lambrecht, Germany,

RRID:SCR_000034). The standard extracellular solution was composed of (mM) 120 NaCl, 20 Hepes, 4 $MgCl_2$, 5 $CaCl_2$, 5 mg/ml glucose and 1 µM tetrodotoxin (pH 7.3). The patch-clamp electrodes (3–5 MΩ) were coated with dental wax, and then filled with an internal solution containing (mM) 95 Cs D-glutamate, 23 HEPES, 30 CsCl, 8 NaCl, 1 $MgCl_2$, 2 Mg-ATP, 0.3 Li-GTP, and 0.5 Cs-EGTA (pH 7.2). The holding potential of -80 mV was not corrected for junction potentials, and the recorded cells were discarded when the leak current measured at this holding potential was bigger than −10 pA, or when series resistance was bigger than 12 MΩ. The cell capacitance (Cm) was measured continuously during the experiments by application of the sine+dc method (Gillis 1995) implemented through the lock-in extension of Patchmaster, using a sinusoidal voltage (800 Hz, 60 mV peak to peak) added to the holding potential. The application of the sinusoidal voltage was suspended from 10 ms before to 10 ms after the end of the depolarizations applied to stimulate the cells.

The exocytosis was induced by a single 5 ms square depolarizations from the holding potential of -80 to -10 mV, or by an action potential-like stimulus (APls), composed by a 2.5 ms ascendant voltage ramp from -80 to +50 mV, followed by a 2.5 ms descendant ramp. In some cells, immediately after the application of a depolarization pulse, we noted the presence of a brief transient capacitance change, probably associated to sodium channels gating (Horrigan & Bookman 1994). This transient became negligible in less than 50 ms after the end of depolarization (Moya-Diaz *et al.* 2016; Chow et al. 1996; Gong et al. 2005). Therefore, to avoid any influence of this fast capacitance transient, the synchronous increase in Cm (ΔCm_{exo}) associated with exocytosis was defined as the difference between the averaged Cm measured in a 50 ms window starting 60 ms after the end of the stimulus minus the average pre-stimulus Cm also measured in a 50 ms window (see the blue segments in Supplementary Figure 1). In a similar way, the following decreased in capacitance (ΔCm_{endo}), associated with endocytosis, was calculated as the difference between the averaged Cm measured in a 50 ms window starting 60 ms after the end of the stimulus minus the averaged Cm measured 5 s after the stimulus, also in a 50 ms window (see the blue segments in Supplementary Figure 1). The Cm decay associated with endocytosis was fitted in each experiment to a single exponential function with the form

($\Delta Cm = Yo + A . e^{-\frac{t}{\tau_{endo}}}$). The data were filtered at 3 kHz. The experiments were carried out at room temperature (22–24◦C).

Amperometric Recordings

Catecholamine release events were measured by amperometry as previously described (González-Jamett et al., 2017) using 5 µm diameter carbon fibers (Thornel P-55; Amoco Performance Product, Greenville, USA) which were held at a potential of +650 mV with HEKA EPC10 amplifier (HEKA Elektronik, Lambrecht/Pfalz, Germany). Cells were maintained in Krebs-HEPES solution (in mM: 140 NaCl, 5.9 KCl, 1.2 MgCl2, 2 CaCl2, 10 HEPES-NaOH, 10 glucose, pH 7.4) throughout the recordings, and exocytosis was induced with a 10 s of the nicotinic agonist dimethylphenylpiperazinium (DMPP) at 50 µM by using a custom-made picospritzer using a pressure of 2-3 psi. Amperometric signals were low pass filtered at 1 kHz and digitized at 5 kHz with the HEKA EPC10 amplifier and the PatchMaster software (HEKA Elektronik, Lambrecht/Pfalz, Germany). Each recording lasted 100 s and was analyzed using a custom-written macro for IGOR PRO (Wavemetrics Inc., Lake Oswego, Oregon, USA) gratefully obtained from Dr. R. Borges (Universidad de Tenerife, Spain). Analyses were restricted to spikes with amplitudes ≥ 10 pA, foot amplitudes ≥ 3 pA and foot durations ≥ 3 ms.

Expression of Neuropeptide Y fused to mCherry as vesicle marker

Chromaffin cells were co-transfected with the construct NPY-mCherry together with Dyn-2 WT, or alternatively Dyn-2 p.A618T or Dyn-2 p.S619L. After 48 hours of transfection, cells were washed (x3) with PBS buffer, where one set of cells served as an unstimulated control, while the other was stimulated with the agonist DMPP (50 µM, 10 s). Then, the cells were fixed in a PBS solution containing 4% saccharose. After 24 h, cells were washed again with PBS and incubated for 10 min with PBS containing tris(hydroxymethyl)aminomethane (10 mM) to deactivate PFA innate fluorescence. Finally, after a final wash (PBS x5), cells were covered with montage liquid Mowiol® and storaged at 4ºC.

Confocal images were obtained with a FV300 (OLYMPUS) confocal microscopy, using a Plan-Apochromat 60x/1.4 Oil DIC objective (OLYMPUS). To visualize the green-fluorescent

marker EGFP, excitation was performed at 488 nm and the emission recorded at 500-520 nm; and for the mCherry red-fluorescent marker, excitation was applied at 543 nm and emission was collected at 600-620 nm. Images were acquired in X, Y and Z axes. In the Z axis, Z-stacks were used, with stacks being separated 0.35 μm from each other.

Images were analyzed in the equatorial plane by using a custom macro on Image J software (NIH, USA). The macro identified masks which accounted for the total and peripheral (1 μm width aligned with the border) areas, using as reference the area occupied by the fluorescence emitted for the EGPF-Dyn-2. Then, a second mask identified the area occupied by the fluorescence of the NPY-mCherry. Percentages of total and peripheral NPY were computed per cell as a ratio between the area associated to NPY-mCherry fluorescence and the cell´s total or peripheral area, respectively.

Actin filament formation

Formation of actin filaments was carried out as previously described (Olivares et al., 2014). In brief, cultured cells were incubated in a buffer containing 139 mM k- glutamate, 20 mM PIPES, 5 mM EGTA, 2 mM ATP-Mg^{2+}, 20 µM digitonin, 10 µM free Ca^{2+} and 0.3 µM Alexa Fluor 488-G-actin conjugate, at pH 6.6 with. Then, cells were fixed with 4% p-formaldehyde in phosphate buffered saline (pH 7.4), stained with 5 mg/ml 4',6-diamidino-2-phenylindole and visualized using a Nikon C1 Plus laser-scanning confocal microscope (Nikon, Tokyo, Japan). All images were captured at the equatorial plane of the cells, using identical exposure settings between compared samples. Confocal images were analyzed and processed using a custom macro on ImageJ software (NIH, USA). The macro identified masks which accounted for: 1) the total cell´s area, using as reference the area associated to mCherry-Dyn-2 fluorescence, determined by Otsu's thresholding algorithm; and 2) the area occupied by Alexa Fluor 488 fluorescence conjugate above a threshold determined by Renyi´s entropy based algorithm, a common standardized technique supported by ImageJ. Finally, the percentage of total F-actin formation was computed per cell as a ratio between Alexa Fluor 488 and mCherry-Dyn-2 associated areas.

Statistics analysis

For every experimental condition, the data (one measurement per cell, and one cell per petry dish) were obtained from several cell cultures, which number is mentioned in every experimental condition. No blinding was performed in this study, and no randomization procedures were applied. No test for outliers was performed. Normality was assessed with Shapiro-Wilk and D'Agostino test. Normally distributed data were analyzed by Student's "t" test (two-tailed) for comparisons between two groups of independent data samples, and by one way ANOVA (two-tailed test) for multiple independent data samples. After ANOVA, Bonferroni test (one-tailed) was used for comparisons between groups. Non-normally distributed data were analyzed using the Mann-Whitney test, or the Kruskal-Wallis test followed by Dunn's post hoc test when pertinent. All statistical analyses were performed using Prism software version (GraphPad V5 Software Inc., La Jolla, CA, USA). To fit endocytosis records we used the nonlinear curve-fitting option in Origin Pro 8 (Microcal Software, RRID:SCR_002815). Data are expressed as means ± SEM for normal distributions. For non-normally distributed data, box plots were used showing a centered, inferior and superior lines, representing the median, first and third quartile, respectively. Top and bottom whiskers lines show the maximum and minimum values of each distribution, respectively.

Materials

ATP-Mg (CAT No: A9187-100MG), Bovine serum albumin (CAT No. 05470-25G), $CaCl_2$ (Cat No: 1.02382.1000), cytosine-1-beta-D-arabinofuranoside (CAT No: C6645-25MG), 4',6-diamidino-2-phenylindole (DAPI) (CAT No: D9542), Digitonin (CAT No: D141-100MG), 1,1-Dimethylphenyl-4-phenilpiperazinium iodide (DMPP) (CAT No: D5891), EGTA (CAT No: E4378-10G), Glucose (Cat No: 1.08337.1000), GTP-Li (CAT No: G5884-25MG), KCl (CAT No: 1.04936.1000), MgCl2 (CAT No: 1.05833.0250), Mowiol® 4-88 (CAT No: 81381-50G), NaCl (CAT No: 1.0604.1000), P-formaldehyde in phosphate (CAT No: 158127-3KG), PIPES (CAT No: P-6757), and poly-L-lysine (CAT No: P8920-100ML) were obtained from Sigma-Aldrich (St. Louis MO USA); Dulbecco's modified Eagle's medium (CAT No: 10567-014), Fetal bovine serum (CAT No:16000-044), gentamycin (CAT No: 15750078), trypsin inhibitor (CAT No:

R007100), and penicillin/streptomycin (CAT No: 15140122) from Gibco (Grand Island, NY USA); tetrodotoxin citrate (CAT No. T-550) from Alomone Labs (Jerusalem, Israel); Collagenase B (CAT No: 11088815001) from Roche; CsCl (CAT No: 102039) from Supelco - Merck (Darmstadt, Alemania); monoclonal anti-dynamin antibody (CAT No: 610246, RRID:AB_397641) from BD Biosciences (San Jose, CA, EEUU); Percoll (CAT No: 17-0891-02) from GE Healthcare (Uppsala, Sweden), and Alexa Fluor 488-G-actin (CAT No: A12373) from Thermo Fisher Scientific (Waltham, MA, USA)

Ethics statement

All research undertaken had the approval of Bioethics (identification numbers BEA080 of Universidad de Valparaíso, Chile; and protocol 168 of the Facultad de Ciencias Exactas y Naturales, Universidad de Buenos Aires). This investigation comprises the use of bovine adrenal glands that were attained from local slaughterhouses: Frigorific Don Pedro, certificated (Livestock role 04.2.03.0002) by the Servicio Agrícola y Ganadero de Chile, and Frigorífico Cocarsa-Ecocarnes S.A., San Fernando, Provincia de Buenos Aires, Argentina, certified by the Servicio Nacional de Sanidad y Calidad Agroalimentaria de Argentina.

The data that support the findings of this study are available from the corresponding authors upon reasonable request.

RESULTS

Dynamin-dependent and dynamin-independent endocytosis induced by depolarization pulses in bovine adrenal chromaffin cells.

In this study, we employed bovine chromaffin cells as our research model. These cells offer unique advantages for studying exocytosis and endocytosis with high temporal resolution, through electrophysiological and electrochemical techniques. Specifically, we focused on dynamin-2, a crucial isoform responsible for regulating exocytosis and endocytosis (González-Jamett et al., 2013a). In the results described below we sought to shed light on the effects of CNM-associated dynamin-2 mutations, A618T and S619L, on exocytosis and endocytosis in chromaffin cells.

Previously, we demonstrated in murine chromaffin cells that the application of short stimuli, particularly a single action potential-like stimulus (APls) or 5 ms square depolarization, activate a fast dynamin-dependent endocytosis, while longer stimuli (10 to 50 ms square depolarizations) induce a fast dynamin-independent endocytosis (Moya-Díaz 2016; Montenegro 2021; Bayonés 2022b). Here, we applied APls and 5 ms square depolarization to study the effect of CNM associated dynamin-2 mutations p.A618T and p.S619L on endocytosis in bovine chromaffin cells. As we mentioned, prior research was done in murine cells, so we first had to characterize the exocytotic and endocytotic responses elicited by the application of the same stimulation protocol, and their dependence on dynamin, in bovine chromaffin cells. Supplementary Figure 2 shows examples of Ca^{2+} currents (Fig. S2 A) and summarizes the Ca^{2+} currents amplitudes (I_{Ca2+}) and integrals ($\int I_{Ca2+}$) (Fig. S2 B & C) obtained in response to the application of a APls and square depolarization pulses of 5 ms (named from now on as 5ms), respectively, in control conditions and in cells dialyzed with a monoclonal antibody against dynamin (Anti-Dyn). In addition, Figure 1 represents typical capacitance recordings obtained in response to the application of both types of depolarizations (Fig.1 A), and a summary of the different parameters associated to exocytosis and endocytosis obtained from the same experiments (Fig.1 B to E). In control conditions, similarly to murine cells (Bayonés et al., 2022b), bovine cells did not exhibit appreciable differences in $\int I_{Ca2+}$, exocytosis (ΔCm_{exo}), or endocytosis

(ΔCm_{endo}). Additionally, also resembling murine cells, there were no effects of Anti-Dyn on I_{Ca2+}, $\int I_{Ca2+}$, or ΔCm_{exo}. More important, as shown in murine cells, ΔCm_{endo} and consequently endo/exo (which represents the efficiency of endocytosis computed as the ratio between ΔCm_{endo} and ΔCm_{exo}) suffered a significant reduction when APls and 5ms were applied in the presence of Anti-Dyn (Figure 1 B, C & D). Lastly, as well as murine cells, the time constant of endocytosis (τ_{endo}) was found to increased (indicating deceleration of endocytosis) in response to Anti-Dyn for APls and 5ms (Figure 1E). Overall, these findings provide valuable insights into the behavior of bovine cells in terms of fast endocytosis and its dependence with dynamin, confirming their similarity to what was described before in murine chromaffin cells.

Dynamin-2 p.A618T and p.S619L mutations inhibited dynamin-dependent endocytosis, but not dynamin-independent endocytosis, in adrenal bovine chromaffin cells.

Subsequently, we proceeded to examine the impact of p.A618T and p.S619L mutations on endocytosis elicited by the aforementioned stimulation protocols. Figure 2A presents examples of capacitance measurements obtained from chromaffin cells expressing, separately, EGFP-wild-type (WT)-dynamin-2 or p.A618T or p.S619L, in response to the application of APls and 5ms. I_{Ca2+}, $\int I_{Ca2+}$ (Fig.S3 B & C) and ΔCm_{exo} (Fig.2 B) were not affected by either of the mutants. Conversely, the expression of both mutants significantly decreased ΔCm_{endo} and the efficiency parameter endo/exo when the cells were stimulated by APls or 5ms (Fig 2C and D). Finally, the rate of endocytosis under the expression of any of both mutants increased their time constant τ (i.e., endocytosis was decelerated) for both type of stimuli (Fig 2E). In conclusion, the effects of p.A618T or p.S619L expression were comparable to the Anti-Dyn treatment, decreasing specifically the magnitude and rate of dynamin-dependent endocytosis induced by short depolarizations.

Dynamin-2 p.A618T and p.S619L mutations inhibited massive exo and endocytosis in adrenal bovine chromaffin cells.

Next, we evaluated the effects of p.A618T and p.S619L on the exocytosis and endocytosis induced by a longer stimulus, such as a 500 ms square depolarization, which forces the

mobilization and release of a bigger number of vesicles. Different authors found that such long depolarizations induce strong exocytosis followed by robust compensatory endocytosis or, alternatively, excess membrane retrieval (Engisch and Nowycky, 1998; Smith and Neher, 1997). In our hands, under the WT condition, this type of stimulation always induced a strong exocytosis followed by a slow compensatory endocytosis (Fig.3A). Notably, the expression of both mutants dramatically decreased the aforesaid parameters related with exocytosis (ΔCm_{exo}), endocytosis (ΔCm_{endo}) and endocytosis efficiency (endo/exo) (Fig.3 B, C and D). On the other hand, I_{Ca2+} and $\int I_{Ca2+}$ evoked by this stimulus were not affected by the expression of the mutants (Fig. S4 B, and C), which points towards that the observed reductions in exocytosis and endocytosis are not associated with alterations in calcium entry. The almost complete abolishment of endocytosis in cells transfected with p.A618T and p.S619L suggest that this process is associated to a dynamin-dependent mechanism, as was suggested by previous studies (Engisch and Nowycky, 1998). In addition, the huge inhibition of ΔCm_{exo} observed in these conditions, together with the lack of effect of p.A618T and p.S619L on this parameter for short depolatizations, suggest that both mutants affect a process that becomes important when exocytosis exceeds a certain number of vesicles.

Dynamin-2 p.A618T and p.S619L Mutations Reduce the Secretion induced by a nicotinic agonist in adrenal bovine chromaffin cells

Bovine chromaffin cells constitute a classical experimental model to study neurosecretion, a cellular process that is also influenced by dynamin-2 (González-Jamett et al., 2013a). Therefore, to analyze the effects of the p.A618T and p.S619L on exocytosis using a different technique and a more physiological approach, we evaluated the release of catecholamine induced with the activation of nAChRs using carbon fiber amperometry. The exocytosis was evoked by a 10 s pulse of the nAChRs agonist DMPP applied to chromaffin cells expressing alternatively EGFP-WT-dynamin-2, or A618T, or S619L. Examples of typical recordings are represented in Figure 4A. As shown in Figure 4B, the number of DMPP-induced exocytotic events was significantly reduced by both mutations, as compared with those expressing EGFP-WT-dynamin-2.

Amperometry also allows the analysis of the dynamics of catecholamines release from individual exocytosis events (Mosharov and Sulzer, 2005). To determine whether A618T or S619L affect the characteristics of the individual exocytotic events, we further analyzed different spike parameters (cartoon on Fig. 4 A), particularly the spike charge (Q), that is proportional to the amount of catecholamines released during each individual event, the spike amplitude, which accounts for the height of the spike, and time elapsed at spike´s half amplitude (HAT). The latter is related to the duration of the release event through an expanded fusion pore (Fang et al., 2008). These parameters where not modified by the expression of A618T or S619L mutations when compared against WT (Fig. 4 C). As the mutations did not modified Q but reduced the number of DMPP-induced exocytotic events, the cumulative Q along experimental time (ΣQ), which is a measurement of the total catecholamine release, was markedly reduced by both mutants (Fig. 4D).

In addition, we also analyzed the amplitude and the duration of the pre-spike foot signal (PSF; Fig. S5 B), which respectively reflect the conductance and stability of the fusion pore (Lindau and Alvarez de Toledo, 2003). The fusion pore is an unstable channel formed during the fusion process (Marengo and Cárdenas, 2017). As shown in the supplementary Figure 5, C and D, neither A618T nor S619L mutation significantly changed these fusion pore parameters.

Dynamin-2 p.A618T and p.S619L Mutations Reduce cortical NPY labeled vesicles in adrenal bovine chromaffin cells

A possible explanation for the effect of both mutations on exocytosis might be the reduction of vesicles available for fusion. It is well known that dynamin activity modulates actin dynamics (Zhang et al., 2020), and actin is involved in the transport of vesicles to plasma membrane (Gimenez-Molina et al., 2018). In consequence, if the expression of p.A618T and p.S619L affect actin dynamics, it is possible that these mutations may disrupt the trafficking of vesicles to the plasma membrane. To assess this hypothesis, we co-expressed NPY-mCherry together with WT dynamin, or p.A618T or p.S619L, fixed the cells, and evaluated the area covered by NPY associated fluorescence by confocal microscopy (see Materials and Methods for more details). It is important to mentioned that NPY is normally localized in

the core of secretory vesicles in physiological conditions (Hwang et al., 2007). We performed these experiments in control rest conditions or after stimulating the cells with 50 µM de DMPP for 10 s before fixation.

Figure 5 (top) show examples of confocal images of cells expressing WT, p.A618T or p.S619L in unstimulated (Fig. 5A) and stimulated conditions (Fig. 5B). It is possible to observe the distribution of NPY (red) throughout the cytosol, and particularly in localized spots in the cell border, probably representing vesicles or vesicle clusters. Dynamin-2 constructs (green) were also distributed throughout the cytosol, and for both mutants it is possible to note the accumulation of fluorescence in big spots, possibly representing mutated dynamin polymers as it was described previously (Wang et al, 2010). The bottom of Figure 5 displays the quantification of the area covered by NPY associated fluorescence in the whole cell (% NPY Total) and in a ring of 1 µm from the cell border (% NPY Periphery), and the ratio between these two areas (% Periphery/Total). The expression of both mutants did not alter any of these parameters in unstimulated cells. However, both mutants decreased very significantly the NPY in the periphery of stimulated cell. These results indicate that the expression of p.A618T or p.S619L impairs the recruitment of secretory vesicles to the cell surface after exocytosis-induced stimulus.

Dynamin-2 p.A618T and p.S619L mutations disturb F-actin dynamics.

It is well known that endocytosis and exocytosis are influenced by actin dynamics (Grassart et al., 2014; Gabel et al., 2015; Cárdenas et al., 2022; Montenegro et al, 2021), and that A618T and S619L mutations disrupt the formation of actin filaments (F-actin) in skeletal myoblasts (Bayonés et al., 2022a). In consequence, we decided to analyze the effect of these mutations on actin dynamics in bovine chromaffin cells. With this goal in mind, we transfected chromaffin cells with mCherry WT, or A618T or S619L dynamin-2. F-actin *de novo* polymerization was evaluated 48 h later by incubating permeabilized chromaffin cells in presence of Alexa Fluor 488-tagged actin monomers (see Materials and Methods for the details of the incubation solution). In this assay, the fluorescence signal corresponds to the recently formed actin filaments (González-Jamett et al., 2013a; González-Jamett et al., 2017); therefore, the percentage of F-actin formation was computed as a ratio between the

area occupied by fluorescent F-actin and cell´s total area (see Methods for further details). As shown in the examples represented in Figure 6A and in the quantification of Figure 6B, both dynamin-2 mutations significantly reduced the formation of new actin filaments.

DISCUSSION

Dynamin-2 was classically associated to endocytosis, however it has also been implicated in other cellular processes, like vesicle trafficking, exocytosis, and regulation of actin filament dynamics (González-Jamett et al., 2013b). Recently, by using total internal reflection fluorescence microscopy in immortalized human myoblasts, we reported that p.A618T and p.S619L dynamin-2 mutations impairs Ca^{2+}-induced exocytosis of GLUT4 containing vesicles (Bayonés et al, 2022a). These two mutations have been linked to severe neonatal forms of CNM (Böhm et al., 2012), a form of skeletal muscle hereditary disease. However, since dynamin-2 is ubiquitously present in a wide variety of tissues (Cao et al, 1998), it is possible that these mutations, which cause a severe neonatal phenotype, may also affect other cell types, including neuroendocrine cells and neurons. In this work we analyze if the CNM associated mutations p.A618T and p.S619L alter exocytosis and endocytosis in chromaffin cells, a classical model for the study of neurosecretion.

Our study shows that both mutations inhibit specifically: (1) a form of dynamin dependent endocytosis that is activated after the application of brief single depolarizations (Bayonés et al, 2022b); (2) the exocytosis and endocytosis triggered by prolonged 500 ms depolarizations; (3) the catecholamine release triggered by the nicotinic pathway activation; and (4) NPY labeled vesicle recruitment to the cell cortex; and finally (5) the *de novo* formation of F-actin filaments.

We wondered if there is a common factor that might explain so many processes affected by these dynamin-2-mutants. It was described in numerous publications that alterations in actin dynamics affect both exocytosis and endocytosis in different systems (Miklavc and Frick, 2020; Wu and Chan, 2022). In this regard, it was shown by several authors, starting three decades ago, that interfering in actin polymerization/depolymerization dynamics affect secretory vesicles transport to plasma membrane, and consequently exocytosis (Trifaró et al., 2002; Meunier and Gutiérrez, 2016; Gutiérrez and Villanueva, 2018). Some investigators have shown that actin filaments are also involved in the mechanism of fusion itself (Doreian et al., 2008; Berberian et al., 2009; Wen et al., 2016). Finally, it was demonstrated that actin filaments also participate in several endocytosis mechanisms, as

bulk endocytosis, classical clathrin-mediated endocytosis, and ultrafast endocytosis (Boulant et al., 2011; Watanabe et al., 2013; Gormal et al., 2015). Particularly, we showed recently that the dynamin-dependent endocytosis induced after short depolarizations, like the one shown in the first section of this paper, is also dependent on polymerized F-actin (Montenegro et al. 2021). In the present work, we observed that p.A618T and p.S619L mutations disrupt the formation of actin filaments in chromaffin cells, and very recently we described a similar effect of both mutations in immortalized human myoblasts (Bayonés et al, 2022a). It is important to note that, from the beginning, dynamin was associated with actin dynamics (Gu et al., 2010; Zhang et al., 2020). It is therefore possible that the disruption of actin filaments formation might be responsible of the effects of these dynamin-2 mutation on endocytosis and neurosecretion.

Other dynamin-2 mutations that cause CNM, such as the mutants R369W and R465W, or mutations linked to Charcot-Marie-Tooth neuropathy like the K562E, also lead to aberrant actin dynamics (Yamada et al., 2016b; González-Jamett et al., 2017; Hamasaki et al. 2022; Arriagada-Diaz et al., 2023). Interestingly, the R465W mutation further perturbs the synaptic plasticity and cognitive function in a mouse model of CNM (Arriagada-Diaz et al., 2023), supporting the pleiotropic role of these mutations. Why these mutations that seem to display increased GTPase activity (Kenniston and Lemmon, 2010) disrupt actin dynamics? A possible explanation is that the enhanced self-assemble of the CNM mutations (Kenniston and Lemmon, 2010; Wang et al., 2010) that lead to the accumulation of large oligomers in the cytosol (James et al., 2014; González-Jamett et al., 2017) renders dynamin less able to interact with F-actin upon a stimulus. The augmented self-assemble of the CNM mutations can also result in the formation of abnormal clathrin-containing structures at the plasma membrane (James et al., 2014) with altered internalization (Ali et al., 2019).

The intricate functions of dynamins, particularly dynamin-2, and the detrimental consequences of disease-associated mutations underscore the critical role of these proteins in cellular homeostasis and disease pathogenesis. Thus, by elucidating the impact of specific mutations on endocytosis, neurosecretion, and cytoskeletal dynamics, this work shed light

on the underlying mechanisms and provide valuable insights into the pathophysiology of centronuclear myopathy.

Acknowledgments

This work was supported by the grants PICT 2764-2016, PICT 02849-2018 and PICT I-A-00176 - 2021 (to FDM) from the Agencia Nacional de Promoción Científica y Tecnológica (Argentina), and FONDECYT 1220825 (to AMC) from ANID (Chile). LB has now a postdoctoral fellowship (# 838783) from CONAHCYT México. We thank CONAHCYT, and Dr. Román Rossi Pool for their positive cooperation during the analysis of data and confection of this manuscript. We also thank to MSc Sergio Parra for helping us with the analysis of amperometry experiments.

Conflict of interest

The authors have no conflicts of interest to declare.

Author Contributions: LB performed experiments, analyzed data, designed and prepared the figures, participated in the writing and revision of the manuscript; MJGF performed experiments and analyzed data, SAB performed experiments; LIG designed and performed analysis of NPY images; CFC performed experiments; XBM performed experiments; AGJ designed experiments and edited the manuscript; AMC conceived the study, designed experiments, and drafted the manuscript; FDM conceived the study, designed experiments, and drafted the manuscript. All authors contributed to interpretation of data and revised the final version of the manuscript. All authors have read and agreed to the published version of the manuscript.

FIGURE LEGENDS

Figure 1. Anti-Dyn suppresses dynamin-dependent endocytosis evoked by action potential like-stimulus and short square depolarizations. (A) Representative examples of Cm recordings in response to the application of APls and 5ms stimuli obtained from two independent cells, where one was dialyzed with standard internal solution for 5 min (control, gray) and the other with a dynamin antibody (Anti-Dyn, red) also for 5 min. The plots in (B), (C), (D) and (E), represent the average values, standard errors, and individual measurements (one measurement/cell) of exocytosis (ΔCm_{exo}), endocytosis (ΔCm_{endo}), ratio between endocytosis and exocytosis (endo/exo), and time constant of endocytosis (τ_{endo}), respectively, obtained by application of APls and 5ms square depolarizations in control (grey) and Anti-Dyn (red) conditions. Data were analyzed by Student's 't' test ((C): APls ($t[12] = 2.479$, $p = 0.029$), 5ms ($t[10] = 2.874$, $p = 0.0166$); (D): APls ($t[12] = 5.883$, $p < 0.001$), 5ms ($t[10] = 2.303$, $p = 0.0441$); (E): APls ($t[12] = 4.466$, $p < 0.001$), 5ms ($t[10] = 2.574$, $p = 0.0277$)). *$p < 0.05$, ***$p < 0.001$. These experiments were performed in 21 cells from 5 different cell cultures. The numbers between brackets represent the number of degrees of freedom handled in each comparison.

Figure 2. p.A618T and p.S619L affect dynamin-dependent endocytosis magnitude and dynamics. (A) Representative examples of Cm recordings in response to the application of APls obtained from three independent cells, where one expressed dynamin-2 WT (black), another A618T (green) and the other S619L (blue). The plots in (B), (C), (D) and (E), represent average values, standard errors, and individual measurements (one measurement/cell) of exocytosis (ΔCm_{exo}), endocytosis (ΔCm_{endo}), ratio between endocytosis and exocytosis (endo/exo), and time constant of endocytosis (τ_{endo}), respectively, obtained by application of APls and 5ms square depolarizations, in WT (black), A618T (green) and S619L (blue), conditions. The data was analyzed by one-way ANOVA ((C): APls ($F[2,41] = 14.39$, $p< 0.001$), 5ms ($F[2,40] = 6.432$, $p = 0.0038$); (D): APls ($F[2,41] = 20.12$, $p < 0.001$), 5ms ($F[2,40] = 6.524$, $p = 0.0035$); (E): APls ($F[2,32] = 23.36$, $p < 0.001$), 5ms ($F[2,30] = 6.778$, $p = 0.0037$)). **$p<0.01$, ***$p < 0.001$. These experiments were performed in 46 cells from 7 different cell

cultures. The numbers between brackets represent the degrees of freedom handled in each comparison.

Figure 3. Dynamin-2 mutations A618T and S619L disrupts exocytosis and endocytosis evoked by prolonged stimulation. (A) Representative examples of Cm recordings in response to the application of a 500 ms square depolarization obtained from three independent cells, where one expressed dynamin-2 WT (black), another A618T (green) and the other S619L (blue). The plots in (B), (C) and (D) represent average values, standard errors, and individual measurements (one measurement/cell) of exocytosis (ΔCm_{exo}), endocytosis (ΔCm_{endo}) and ratio between endocytosis and exocytosis (endo/exo), respectively, obtained by application of 500 ms square depolarization, in WT (black), A618T (green) and S619L (blue), conditions. The data was analyzed by one-way ANOVA ((B): $F[2,29] = 12.39$, $p < 0.001$); (C): $F[2,29] = 27.83$, $p< 0.001$); (D): $F[2,29] = 18.78$, $p < 0.001$)). ***$p < 0.001$. These experiments were performed in 31 cells from 5 different cell cultures. The numbers between brackets represent the degrees of freedom handled in each comparison.

Figure 4. Dynamin-2 mutations disrupt secretion provoked by nicotinic agonist long-lasting stimulation. (A) Left: Representative amperometric recordings obtained from three individual cells stimulated with the nicotinic agonist DMPP for 10 s (orange arrow), one expressing dynamin-2 WT (black), another A618T (green) and the other S619L (blue). Right: a representative amperometric spike, displaying a pre-spike foot signal (PFS), extracted from the WT trace on the left (see reference dotted red box). The parameters Q (area under the spike), amplitude (length of the spike from the basal line) and HAT (elapsed time at spike´s half amplitude) are marked in red. (B) The number of spikes per cell (each colored empty circle) is displayed for the three conditions, WT (black), A618T (green) and S619L (blue), in a log10 scale. Cells expressing the mutations p.A618T and p.S619L significantly decreased its response when compared against the WT condition (C) The parameters Q, amplitude, and HAT are displayed in the three conditions, WT (black), A618T (green) and S619L (blue), in a log10 scale. Each empty circle represents the median obtained from the totality of spikes

recorded in each cell. Neither of these parameters are significantly changed between conditions. For (B) and (C), the centered, inferior, and superior lines in the box plot represents the median, and first and third quartiles, respectively. Top and bottom whiskers lines show the maximum and minimum values of each distribution, respectively. (D) Cumulative integration of the Q parameter (ΣQ) for each experimental condition (WT, A618T and S619L). Each individual experiment (one measurement per cell) was binned in intervals of 1 s, all experiments were averaged, and represented as means ± SEM. ΣQ decreased markedly in cells transfected with A618T or S619L. In B and C data was analyzed by using a Kruskal-Wallis test followed by Dunn's multiple comparison test against WT condition, while in D a Kolmogorov-Smirnov test was applied. ***$p < 0.001$. These experiments were performed in 96 cells from 7 different cell cultures.

Figure 5. Dynamin-2 mutations affect vesicle translocation to the plasma membrane in stimulated chromaffin cells. (A) Representative images, taken at the equatorial plane, of three unstimulated (I) or DMPP-stimulated (II) chromaffin cells co-expressing separately the Dyn-2 constructs EGPF-tagged WT (top row), p.A618T (middle row) or p.S619L (bottom row) and the vesicle fluorescent marker NPY-mCherry. Stimulation with 50 µM DMPP lasted 10 s. EGFP fluorescence is represented in the left column (Dyn II), mCherry fluorescence is represented in the middle column (NPY), while the right column depicts the merge of both fluorescence channels. Scale bar = 5 µm. (B) Percentage of the area occupied by NPY-Cherry with respect to the cell´s full area (% NPY Total), or percentage of the area occupied by NPY-Cherry in a peripheral area of 1 µm wide aligned with the plasma membrane (% NPY Periphery), or the ratio % NPY Periphery/% NPY Total, in unstimulated (I) or DMPP stimulated (II) chromaffin cells expressing Dyn-2 WT (black), p.A618T (blue) and p.S619L (violet). Each cell is represented by filled colored dots, while the centered, inferior and superior lines in the box plot represents the median, first and third quartile, respectively. Top and bottom whiskers lines show the maximum and minimum values of each distribution, respectively. In unstimulated cells, no differences were found among the three conditions for all calculated parameters. On the other hand, for stimulated cells, %NPY

Periphery and the ratio % Periphery/Total drastically decreased for those cells expressing the mutations of Dyn-2. Data in panels A and B was analyzed by using a Kruskal-Wallis test followed by Dunn's multiple comparison test against WT condition. **$p < 0.01$. These experiments were performed in 33 cells from 3 different cell cultures.

Figure 6. Dynamin-2 mutations impaired *de novo* F-actin formation in chromaffin cells. (A) Representative images of three independent chromaffin cells expressing Dyn-2 WT (top row), or p.A618T (middle row) or p.S619L (bottom row). The columns show (from left to right) the expression of Dyn-2 fused to the mCherry fluorescent marker (mCherry column); the F-actin *de novo* formation, assessed by incubating the transfected cells with a G-actin Alexa Fluor 488 conjugate (F-actin column); the nucleus, stained with DAPI fluorescent probe (DAPI column); and the merging of the three previous channels. Scale bar = 5 μm. (B) The F-actin *de novo* formation per cell (empty colored circles), computed as the ratio (%) between the area occupied by Alexa Fluor 488 F-actin fluorescence and cell´s full area (see Methods), are shown for WT (black), A618T (orange) and S619L (pink). The centered, inferior and superior lines in the box plot represents the median, first and third quartile, respectively. Top and bottom whiskers lines show the maximum and minimum values of each distribution, respectively. The mutations p.A618T and p.S619L notably decreased the F-actin *de novo* formation when compared against the WT condition. Data in B was analyzed by using a Kruskal-Wallis test followed by Dunn's multiple comparison test against WT condition. ***$p < 0.001$. These experiments were performed in 35 cells from 4 different cell cultures.

REFERENCES

Ali, T., Bednarska, J., Vassilopoulos, S., Tran M, Diakonov, I.A., Ziyadeh-Isleem, A., Guicheney, P., Gorelik, J., Korchev, Y.E., Reilly, M.M., Bitoun, M., & Shevchuk, A. (2019). Correlative SICM-FCM reveals changes in morphology and kinetics of endocytic pits induced by disease-associated mutations in dynamin. FASEB Journal 33(7):8504-8518. doi: 10.1096/fj.201802635R.

Arriagada-Diaz, J., Prado-Vega, L., Cárdenas Díaz, A.M., Ardiles, A.O., & Gonzalez-Jamett, A.M. (2020). Dynamin Superfamily at Pre- and Postsynapses: Master Regulators of Synaptic Transmission and Plasticity in Health and Disease. Neuroscientist. Dec 10:10738584209743requiered13. doi: 10.1177/1073858420974313.

Arriagada-Diaz, J., Flores-Muñoz, C., Gómez-Soto, B., Labraña-Allende, M., Mattar-Araos, M., Prado-Vega, L., Hinostroza, F., Gajardo, I., Guerra-Fernández, M.J., Bevilacqua, J.A., Cárdenas, A.M., Bitoun, M., Ardiles, A.O., & Gonzalez-Jamett, A.M. (2023). A centronuclear myopathy-causing mutation in dynamin-2 disrupts neuronal morphology and excitatory synaptic transmission in a murine model of the disease. Neuropathol Appl Neurobiol 49(4):e12918. doi: 10.1111/nan.12918.

Bayonés. L., Guerra-Fernández, M.J., Hinostroza, F., Báez-Matus, X., Vásquez-Navarrete, J., Gallo, L.I., Parra, S., Martínez, A.D., González-Jamett, A., Marengo, F.D., & Cárdenas, A.M. (2022a). Gain-of-Function Dynamin-2 Mutations Linked to Centronuclear Myopathy Impair Ca2+-Induced Exocytosis in Human Myoblasts. Int J Mol Sci. 23(18):10363. doi: 10.3390/ijms231810363.

Bayonés, L., Alfonso-Bueno, S., Montenegro, M., Moya-Díaz, J., Caspe, O., Gallo, L.I., & Marengo, F.D. (2022b). Membrane retrieval after Immediately Releasable Pool (IRP) exocytosis is produced by dynamin-dependent and dynamin-independent/protein kinase C-dependent mechanisms. Journal of Neurochemistry, 163, 391–405.

Berberian, K., Torres, A.J., Fang, Q., Kisler, K., & Lindau, M. (2009). F-actin and myosin II accelerate catecholamine release from chromaffin granules. J Neurosci. 29(3):863-70. doi: 10.1523/JNEUROSCI.2818-08.2009.

Böhm, J., Biancalana, V., Dechene, E.T., Bitoun, M., Pierson, C.R., Schaefer, E., Karasoy, H., Dempsey, M.A., Klein, F., Dondaine, N., et al. (2012). Mutation spectrum in the large GTPase dynamin 2, and genotype-phenotype correlation in autosomal dominant centronuclear myopathy. Hum. Mutat. 33:949–959. doi: 10.1002/humu.22067.

Boulant, S., Kural, C,. Zeeh, J.C., Ubelmann, F., & Kirchhausen, T. (2011) Actin dynamics counteract membrane tension during clathrin-mediated endocytosis. Nat Cell Biol. 13(9):1124-31. doi: 10.1038/ncb2307.

Cárdenas, A.M., Gallo, L.I., & Marengo, F.D. (2022) Exocytosis, endocytosis and recycling of secretory vesicles in neuroendocrine cells, and its regulation by cortical actin. BioCell 46:1867–1873.

Chanaday, NL, & Kavalali, ET (2018) Optical detection of three modes of endocytosis at hippocampal synapses. eLife 7:e36097. doi: https://doi.org/10.7554/eLife.36097

Chin, Y.H., Lee, A., Kan, H.W., Laiman, J., Chuang, M.C., Hsieh, S.T., & Liu, Y.W. (2015). Dynamin-2 mutations associated with centronuclear myopathy are hypermorphic and lead to T-tubule fragmentation. Hum Mol Genet. 24(19):5542-54. doi: 10.1093/hmg/ddv285.

Chuang, M.C., Lin, S.S., Ohniwa, R.L., Lee, G.H., Su, Y.A., Chang, Y.C., Tang, M.J., & Liu, Y.W. (2019). Tks5 and Dynamin-2 enhance actin bundle rigidity in invadosomes to promote myoblast fusion. J Cell Biol. 218(5):1670-1685. doi: 10.1083/jcb.201809161.

Chow, R. H., Klingauf, J., Heinemann, C., Zucker, R. S., & Neher, E. (1996). Mechanisms determining the time course of secretion in neuroendocrine cells. Neuron, 16, 369–376.

Doreian, B.W., Fulop, T.G., & Smith, C.B. (2008). Myosin II activation and actin reorganization regulate the mode of quantal exocytosis in mouse adrenal chromaffin cells. J Neurosci. 28(17):4470-8. doi: 10.1523/JNEUROSCI.0008-08.2008.

Engisch, K. L., & Nowycky, M. C. (1998). Compensatory and excess retrieval: Two types of endocytosis following single step depolarizations in bovine adrenal chromaffin cells. The Journal of Physiology, 506(Pt 3), 591–608.

Fang, Q., Berberian, K., Gong, L.W., Hafez, I., Sørensen, J.B., & Lindau M. (2008). The role of the C terminus of the SNARE protein SNAP-25 in fusion pore opening and a model for fusion pore mechanics. Proc Natl Acad Sci U S A. 105(40):15388-92. doi: 10.1073/pnas.0805377105.

Gabel. M., Delavoie. F., Demais, V., Royer, C., Bailly, Y., Vitale, N., Bader, M.F., & Chasserot-Golaz, S. (2015). Annexin A2-dependent actin bundling promotes secretory granule docking to the plasma membrane and exocytosis. J Cell Biol. 210(5):785-800. doi: 10.1083/jcb.201412030.

Gandasi, N.R., Vestö, K., Helou, M., Yin, P., Saras, J., & Barg, S. (2015). Survey of Red Fluorescence Proteins as Markers for Secretory Granule Exocytosis. PLoS One 10(6):e0127801. doi: 10.1371/journal.pone.0127801.

Gillis, K. D. (1995). Techniques for membrane capacitance measurements. In B. Sakmann & E. Neher (Eds.), Single-channel Recording (2nd ed., pp. 155–198). Plenum.

Gimenez-Molina, Y., Villanueva, J., Francés, M.D.M., Viniegra, S., & Gutiérrez, L.M. (2018). Multiple Mechanisms Driving F-actin-Dependent Transport of Organelles to and From Secretory Sites in Bovine Chromaffin Cells. Front Cell Neurosci. 12:344. doi: 10.3389/fncel.2018.00344.

Gong, L. W., Di Paolo, G., Diaz, E., Cestra, G., Diaz, M. E., Lindau, M., De Camilli, P., & Toomre, D. (2005). Phosphatidylinositol phosphate kinase type I gamma regulates dynamics of large dense-core vesicle fusion. Proceedings of the National Academy of Sciences of the United States of America, 102, 5204–5209

González-Jamett, A.M., Momboisse, F., Guerra, M.J., Ory, S., Báez-Matus, X., Barraza, N., Calco, V., Houy, S., Couve, E., Neely, A., Martínez, A.D., Gasman, S., & Cárdenas, A.M. (2013a). Dynamin-2 regulates fusion pore expansion and quantal release through a mechanism that involves actin dynamics in neuroendocrine chromaffin cells. PLoS One 8(8):e70638. doi: 10.1371/journal.pone.0070638.

González-Jamett, A.M., Momboisse, F., Haro-Acuña, V., Bevilacqua, J.A., Caviedes, P., & Cárdenas, A.M. (2013b). Dynamin-2 function and dysfunction along the secretory pathway. Front Endocrinol (Lausanne) 4:126. doi: 10.3389/fendo.2013.00126.

González-Jamett, A.M., Guerra, M.J., Olivares, M.J., Haro-Acuña, V., Baéz-Matus, X., Vásquez-Navarrete, J., Momboisse, F., Martinez-Quiles, N., & Cárdenas, A.M. (2017). The F-Actin Binding Protein Cortactin Regulates the Dynamics of the Exocytotic Fusion Pore through its SH3 Domain. Front Cell Neurosci. 11:130. doi: 10.3389/fncel.2017.00130.

González-Jamett, A.M., Haro-Acuña, V., Momboisse, F., Caviedes, P., Bevilacqua, J.A., & Cárdenas, A.M. (2014). Dynamin-2 in nervous system disorders. J Neurochem. 128(2):210-23. doi: 10.1111/jnc.12455.

Gormal, R.S., Nguyen, T.H., Martin, S., Papadopulos, A., & Meunier, F.A. (2015). An acto-myosin II constricting ring initiates the fission of activity-dependent bulk endosomes in neurosecretory cells. J Neurosci. 35(4):1380-9. doi: 10.1523/JNEUROSCI.3228-14.2015.

Grassart, A., Cheng, A.T., Hong, S.H., Zhang, F., Zenzer, N., Feng, Y., Briner, D.M., Davis, G.D., Malkov, D., & Drubin, D.G. (2014). Actin and dynamin2 dynamics and interplay during clathrin-mediated endocytosis. J Cell Biol. 205(5):721-35. doi: 10.1083/jcb.201403041.

Gu, C., Yaddanapudi, S., Weins, A., Osborn, T., Reiser, J., Pollak, M., Hartwig, J., & Sever, S. (2010). Direct dynamin-actin interactions regulate the actin cytoskeleton. EMBO J. 29(21):3593-606. doi: 10.1038/emboj.2010.249.

Guerra, M.J., González-Jamett, A.M., Báez-Matus, X., Navarro-Quezada, N., Martínez, A.D., Neely, A., & Cárdenas, A.M. (2019). The Ca(2+) channel subunit Ca(V) beta2a-subunit down-regulates voltage-activated ion current densities by disrupting actin-dependent traffic in chromaffin cells. J Neurochem. 151(6):703-715. doi: 10.1111/jnc.14851.

Gutiérrez, L.M., & Villanueva, J. (2018). The role of F-actin in the transport and secretion of chromaffin granules: an historic perspective. Pflugers Arch. 470(1):181-186. doi: 10.1007/s00424-017-2040-9.

Hamasaki, E., Wakita, N., Yasuoka, H., Nagaoka, H., Morita, M., Takashima, E., Uchihashi, T., Takeda, T., Abe, T., Lee, J.W., Iimura, T., Saleem, M.A., Ogo, N., Asai, A., Narita, A., Takei,

K., & Yamada, H. (2022). The Lipid-Binding Defective Dynamin 2 Mutant in Charcot-Marie-Tooth Disease Impairs Proper Actin Bundling and Actin Organization in Glomerular Podocytes. Front Cell Dev Biol. 10:884509. doi: 10.3389/fcell.2022.884509.

Horrigan, F. T., & Bookman, R. J. (1994). Releasable pools and the kinetics of exocytosis in adrenal chromaffin cells. Neuron, 13, 1119–1129.

Hwang, S.R., O'Neill A., Bark, S., Foulon, T., & Hook, V. (2007). Secretory vesicle aminopeptidase B related to neuropeptide processing: molecular identification and subcellular localization to enkephalin- and NPY-containing chromaffin granules. J Neurochem. 100(5):1340-50. doi: 10.1111/j.1471-4159.2006.04325.x.

James, N.G., Digman, M.A., Ross, J.A., Barylko, B., Wang, L., Li, J., Chen, Y., Mueller, J.D, Gratton, E., Albanesi, J.P., & Jameson, D.M. (2014). A mutation associated with centronuclear myopathy enhances the size and stability of dynamin 2 complexes in cells. Biochim Biophys Acta 1840(1):315-21. doi: 10.1016/j.bbagen.2013.09.001.

Kenniston, J.A., & Lemmon, M.A. (2010). Dynamin GTPase regulation is altered by PH domain mutations found in centronuclear myopathy patients. EMBO J. 29, 3054–3067.

Koutsopoulos, O. S., Koch, C., Tosch, V., Böhm, J., North K. N. & Laporte J. (2011). Mild functional differences of dynamin 2 mutations associated to centronuclear myopathy and Charcot-Marie Tooth peripheral neuropathy. PLoS ONE 6, e27498.

Lindau, M., & Alvarez de Toledo, G. (2003). The fusion pore. Biochim Biophys Acta 1641(2-3):167-73. doi: 10.1016/s0167-4889(03)00085-5.

Marengo, F.D., & Cárdenas, A.M. (2018). How does the stimulus define exocytosis in adrenal chromaffin cells? Pflugers Arch. 470(1):155-167. doi: 10.1007/s00424-017-2052-5.

Marie-Anaïs, F., Mazzolini, J., Herit, F., & Niedergang, F. (2016). Dynamin-Actin Cross Talk Contributes to Phagosome Formation and Closure. Traffic 17(5):487-99. doi: 10.1111/tra.12386.

Meunier, F.A., & Gutiérrez, L.M. (2016). Captivating New Roles of F-Actin Cortex in Exocytosis and Bulk Endocytosis in Neurosecretory Cells. Trends Neurosci. 39(9):605-613. doi: 10.1016/j.tins.2016.07.003.

Miklavc, P., & Frick, M. (2020). Actin and Myosin in Non-Neuronal Exocytosis. Cells 9(6):1455. doi: 10.3390/cells9061455.

Montenegro, M., Bayones, L., Moya-Diaz, J., Borassi, C., Martin Toscani, A., Gallo, L. I., & Marengo, F. D. (2021). Rapid vesicle replenishment after the immediately releasable pool exocytosis is tightly linked to fast endocytosis, and depends on basal calcium and cortical actin in chromaffin cells. Journal of Neurochemistry, 157, 1069–1085.

Mosharov, E.V., & Sulzer, D. (2005). Analysis of exocytotic events recorded by amperometry. Nat Methods 2(9):651-8. doi: 10.1038/nmeth782.

Moya-Diaz, J., Alvarez, Y. D., Montenegro, M., Bayones, L., Belingheri, A. V., Gonzalez-Jamett, A. M., Cardenas, A. M., & Marengo, F. D. (2016). Sustained Exocytosis after Action Potential-Like Stimulation at Low Frequencies in Mouse Chromaffin Cells Depends on a Dynamin-Dependent Fast Endocytotic Process. Frontiers in Cellular Neuroscience, 10, 184. doi: 10.3389/fncel.2016.00184.

Nguyen, T.H., Maucort, G., Sullivan, R.K., Schenning, M., Lavidis, N.A., McCluskey, A., Robinson, P.J., & Meunier, F.A. (2012). Actin- and dynamin-dependent maturation of bulk endocytosis restores neurotransmission following synaptic depletion. PLoS One. 7(5):e36913. doi: 10.1371/journal.pone.0036913

Olivares, M.J., González-Jamett, A.M., Guerra, M.J., Baez-Matus, X., Haro-Acuña, V., Martínez-Quiles, N., & Cárdenas, A.M. (2014). Src kinases regulate de novo actin polymerization during exocytosis in neuroendocrine chromaffin cells. PLoS One 9(6):e99001. doi: 10.1371/journal.pone.0099001.

Palmer, S.E., Smaczynska-de Rooij, I.I., Marklew, C.J., Allwood, E.G., Mishra, R., Johnson, S., Goldberg, M.W., & Ayscough, K.R. (2015). A dynamin-actin interaction is required for vesicle scission during endocytosis in yeast. Curr Biol. 25(7):868-78. doi: 10.1016/j.cub.2015.01.061.

Ramachandran, R., Pucadyil, T. J., Liu, Y., Acharya, S., Leonard, M., Lukiyanchuk, V., & Schmid, S.L. (2009). Membrane insertion of the pleckstrin homology domain variable loop 1 is critical for dynamin-catalyzed vesicle scission. Mol. Biol. Cell 20, 4630–4639.

Shin, W., Ge, L., Arpino, G., Villarreal, S.A., Hamid, E., Liu, H., Zhao, W.D., Wen, P.J., Chiang, H.C., & Wu, L.G. (2018). Visualization of Membrane Pore in Live Cells Reveals a Dynamic-Pore Theory Governing Fusion and Endocytosis. Cell 173(4):934-945.e12. doi: 10.1016/j.cell.2018.02.062.

Sidiropoulos, P. N., Miehe, M., Bock, T., Tinelli, E., Oertli, C. I., Kuner, R., Meijer, D., Wollscheid, B., Niemann, A, & Suter, U. (2012). Dynamin 2 mutations in Charcot–Marie–Tooth neuropathy highlight the importance of clathrin-mediated endocytosis in myelination. Brain 135, 1395–1411.

Smith, C., & Neher, E. (1997). Multiple forms of endocytosis in bovine adrenal chromaffin cells. The Journal of Cell Biology, 139, 885–894.

Trifaró, J.M., Lejen, T., Rosé, S.D., Pene, T.D., Barkar, N.D., & Seward, E.P. (2002). Pathways that control cortical F-actin dynamics during secretion. Neurochem Res. 27(11):1371-85. doi: 10.1023/a:1021627800918.

Wang, L., Barylko, B., Byers, C., Ross, J.A., Jameson, D.M. & Albanesi, J.P. (2010). Dynamin 2 mutants linked to centronuclear myopathies form abnormally stable polymers. J. Biol. Chem. 285, 22753–22757.

Watanabe, S., Rost, B.R., Camacho-Pérez, M., Davis, M.W., Söhl-Kielczynski, B., Rosenmund C., & Jorgensen, E.M. (2013). Ultrafast endocytosis at mouse hippocampal synapses. Nature 504(7479):242-247. doi: 10.1038/nature12809.

Wen, P.J., Grenklo, S., Arpino, G., Tan, X., Liao, H.S., Heureaux, J., Peng, S.Y., Chiang, H.C., Hamid, E., Zhao, W.D., Shin, W., Näreoja, T., Evergren, E., Jin, Y., Karlsson, R., Ebert, S.N., Jin, A., Liu, A.P., Shupliakov, O., & Wu, L.G. (2016). Actin dynamics provides membrane tension to merge fusing vesicles into the plasma membrane. Nat Commun. 7:12604. doi: 10.1038/ncomms12604.

Wu, L.G., & Chan, C.Y. (2022). Multiple Roles of Actin in Exo- and Endocytosis. Front Synaptic Neurosci. 14:841704. doi: 10.3389/fnsyn.2022.841704.

Yamada, H., Abe, T., Satoh, A., Okazaki, N., Tago, S., Kobayashi, K., Yoshida, Y., Oda, Y., Watanabe, M., Tomizawa, K., Matsui, H., & Takei, K. (2013). Stabilization of actin bundles by a dynamin 1/cortactin ring complex is necessary for growth cone filopodia. J Neurosci. 33(10):4514-26. doi: 10.1523/JNEUROSCI.2762-12.2013.

Yamada, H., Takeda, T., Michiue, H., Abe, T., & Takei, K. (2016a). Actin bundling by dynamin 2 and cortactin is implicated in cell migration by stabilizing filopodia in human non-small cell lung carcinoma cells. Int J Oncol. 49(3):877-86. doi: 10.3892/ijo.2016.3592.

Yamada, H., Kobayashi, K., Zhang, Y., Takeda, T., & Takei, K. (2016b). Expression of a dynamin 2 mutant associated with Charcot-Marie-Tooth disease leads to aberrant actin dynamics and lamellipodia formation. Neurosci Lett. 628:179-85. doi: 10.1016/j.neulet.2016.06.030.

Zhang, R., Lee, D.M., Jimah, J.R., Gerassimov, N., Yang, C., Kim, S., Luvsanjav, D., Winkelman, J., Mettlen, M., Abrams, M.E., Kalia, R., Keene, P., Pandey, P., Ravaux, B., Kim, J.H., Ditlev, J.A., Zhang, G., Rosen, M.K., Frost, A., Alto, N.M., Gardel, M., Schmid, S.L., Svitkina, T.M., Hinshaw, J.E., & Chen EH. (2020). Dynamin regulates the dynamics and mechanical strength of the actin cytoskeleton as a multifilament actin-bundling protein. Nat Cell Biol. 22(6):674-688. doi: 10.1038/s41556-020-0519-7.

Figure 1

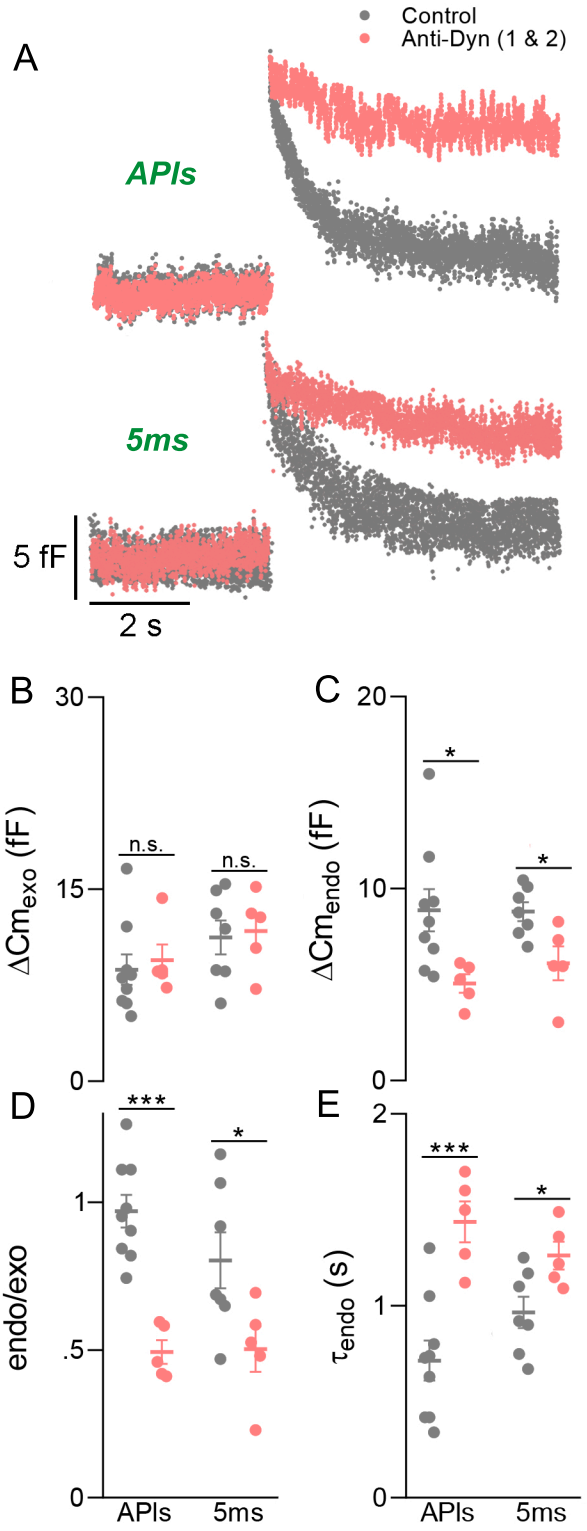
A
Control
Anti-Dyn (1 & 2)
APIs
5ms
5 fF
2 s
B
30
15
0
ΔCm_exo (fF)
n.s.
n.s.
C
20
10
0
ΔCm_endo (fF)
*
*
D
1
.5
0
endo/exo
***
*
E
2
1
0
τ_endo (s)
***
*
APIs
5ms
APIs
5ms

Figure 2

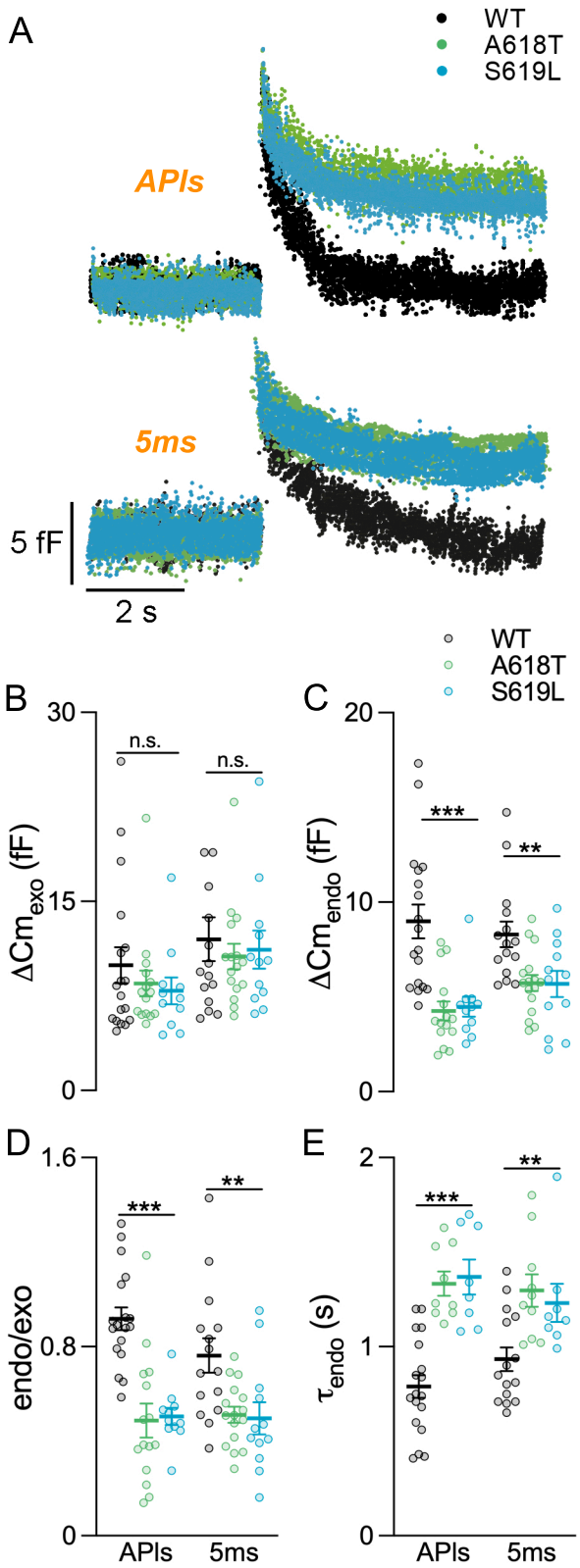
A
WT
A618T
S619L
APIs
5ms
5 fF
2 s
B
C
D
E
n.s.
***
**
ΔCm_exo (fF)
ΔCm_endo (fF)
endo/exo
τ_endo (s)
APIs
5ms

Figure 3

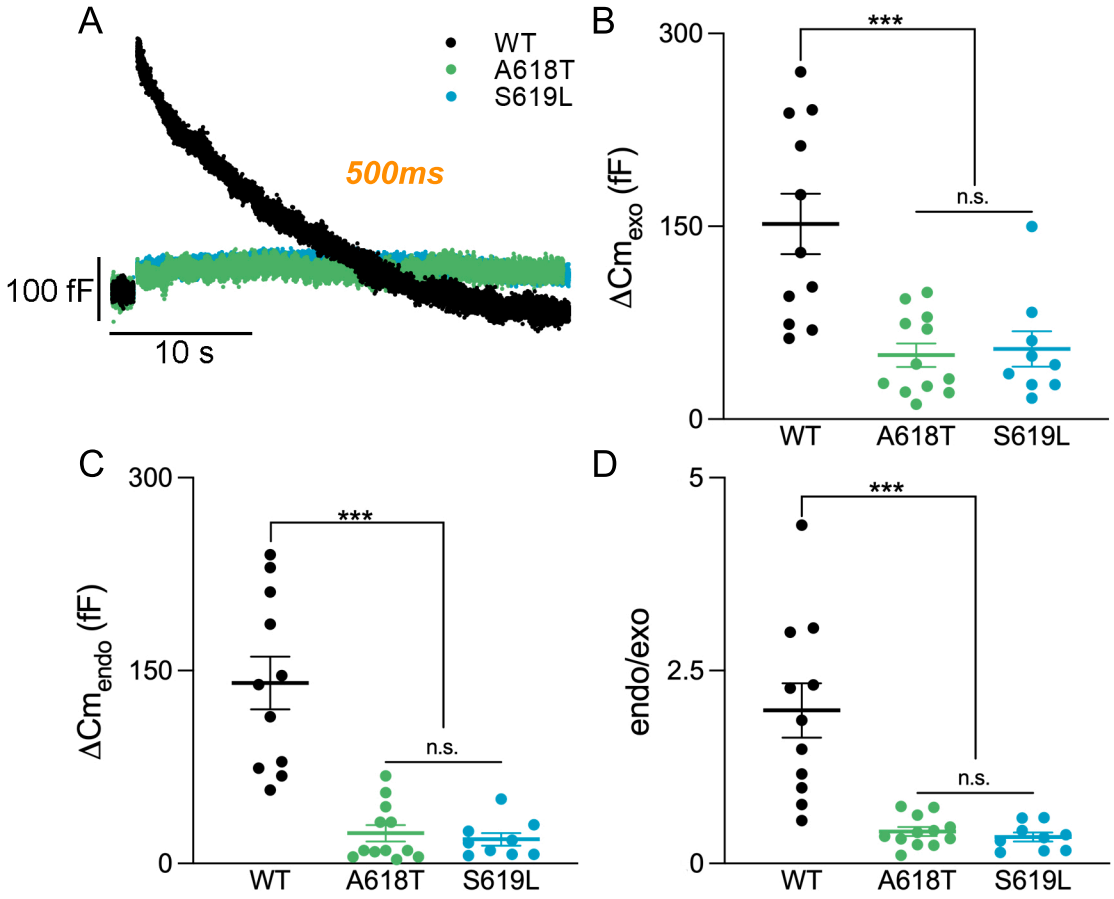
A
WT
A618T
S619L
500ms
100 fF
10 s
B
300
150
0
ΔCm_exo (fF)
***
n.s.
WT
A618T
S619L
C
300
150
0
ΔCm_endo (fF)
***
n.s.
WT
A618T
S619L
D
5
2.5
0
endo/exo
***
n.s.
WT
A618T
S619L

Figure 4

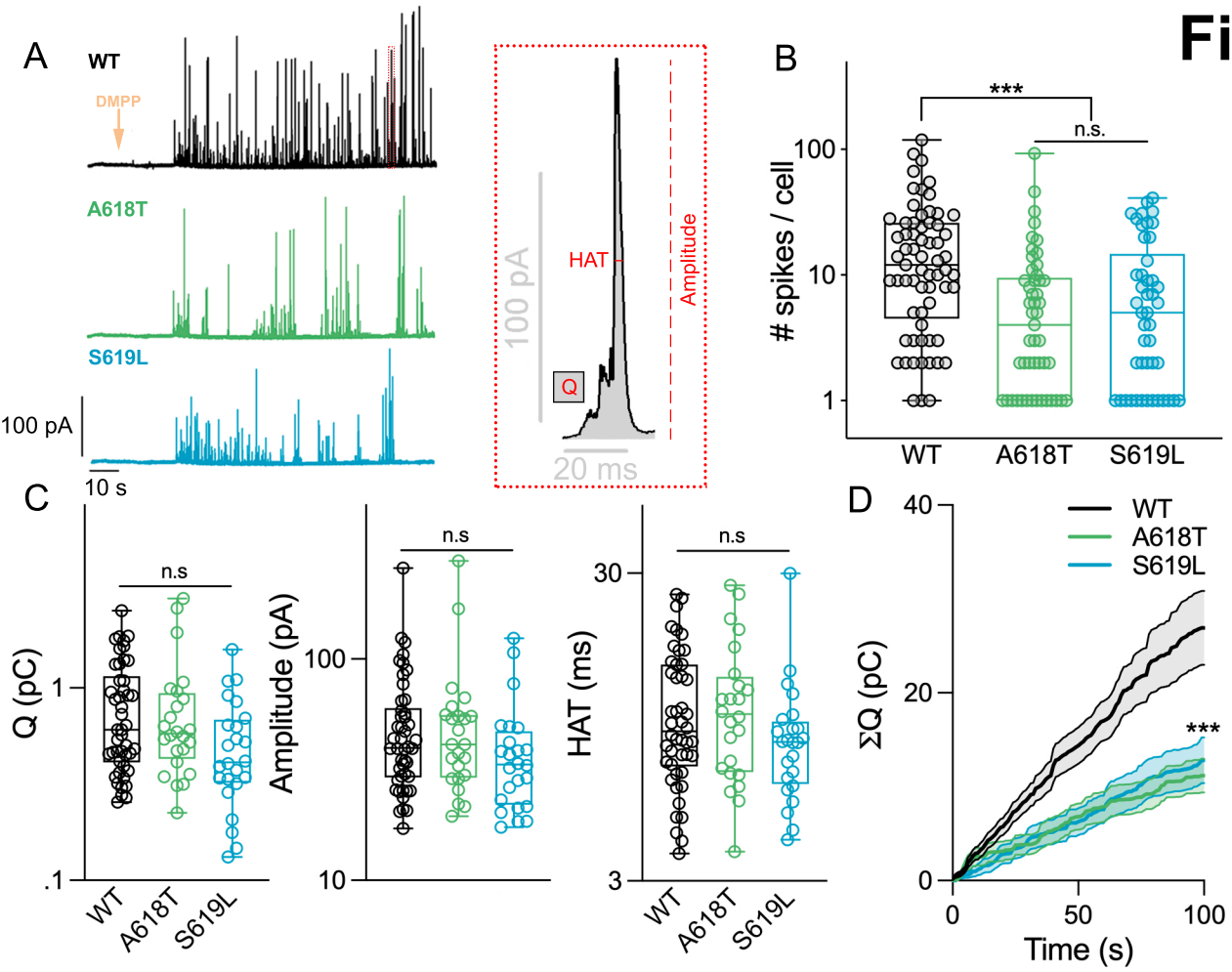
A
WT
DMPP
A618T
S619L
100 pA
10 s
HAT
Q
100 pA
Amplitude
20 ms
B
***
n.s.
spikes / cell
100
10
1
WT
A618T
S619L
C
n.s
Q (pC)
1
.1
WT
A618T
S619L
n.s
Amplitude (pA)
100
10
n.s
HAT (ms)
30
3
WT
A618T
S619L
D
WT
A618T
S619L
ΣQ (pC)
40
20
0
***
0
50
100
Time (s)

Figure 5

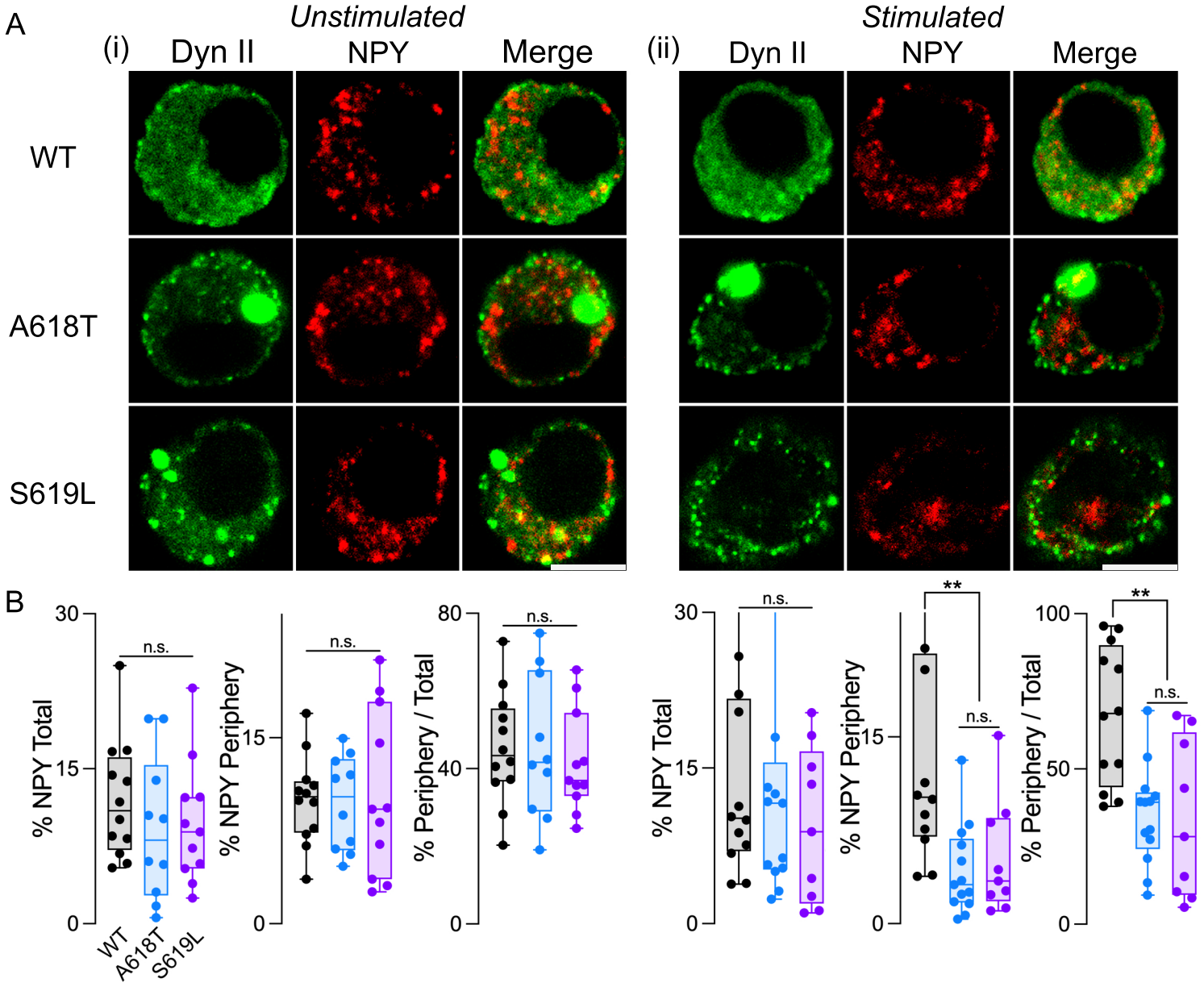
A
(i)
Unstimulated
Dyn II
NPY
Merge
(ii)
Stimulated
Dyn II
NPY
Merge
WT
A618T
S619L
B
% NPY Total
% NPY Periphery
% Periphery / Total
n.s.
**
WT
A618T
S619L

Figure 6

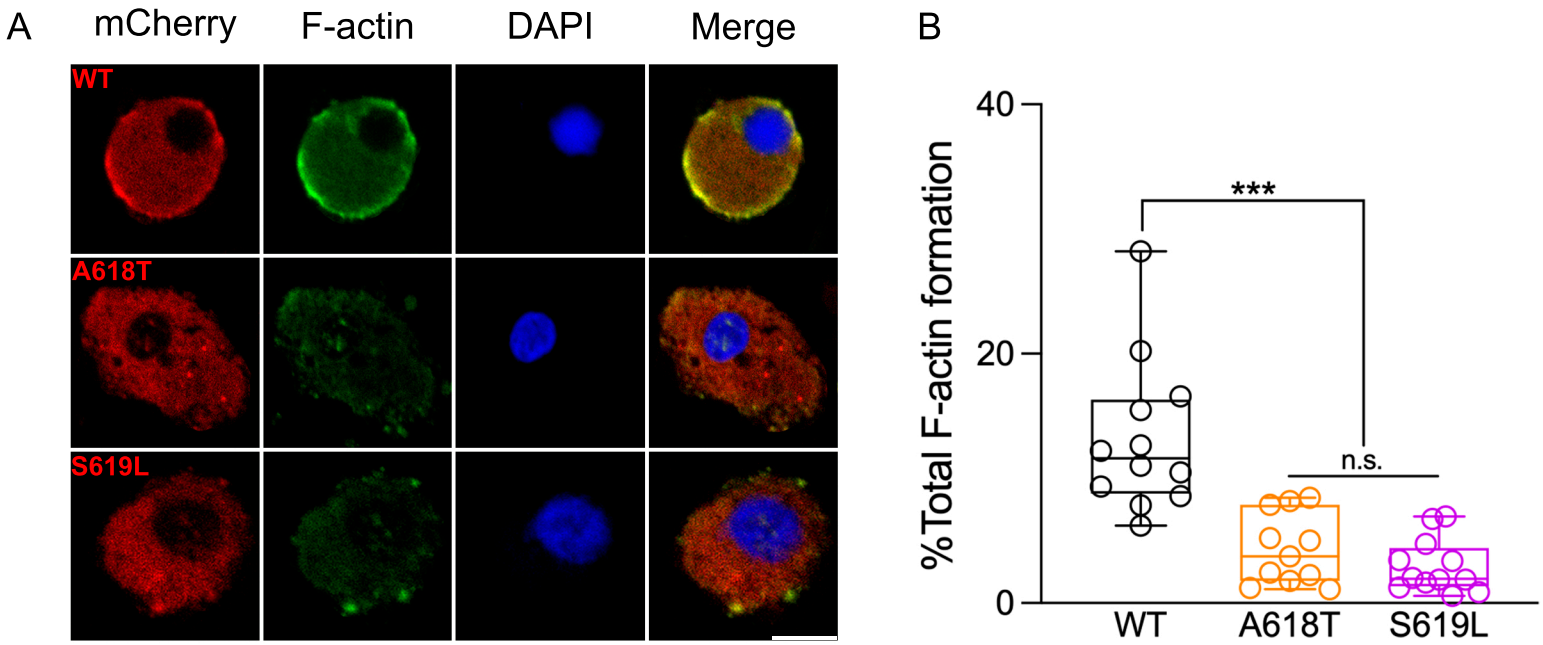
A
mCherry
F-actin
DAPI
Merge
WT
A618T
S619L
B
%Total F-actin formation
40
20
0
***
n.s.
WT
A618T
S619L